3D Volumetric Analysis of Wind Turbine Wake Properties in the Atmosphere Using High-Resolution Doppler Lidar

ROBERT M. BANTA,* YELENA L. PICHUGINA,[+,*] W. ALAN BREWER,* JULIE K. LUNDQUIST,[#,@] NEIL D. KELLEY,[&] SCOTT P. SANDBERG,* RAUL J. ALVAREZ II,* R. MICHAEL HARDESTY,[+] AND ANN M. WEICKMANN[+]

[*] *NOAA/ESRL, Boulder, Colorado*
[+] *Cooperative Institute for Research in Environmental Sciences, Boulder, Colorado*
[#] *University of Colorado Boulder, Boulder, Colorado*
[@] *National Renewable Energy Laboratory, Golden, Colorado*
[&] *Boulder, Colorado*

(Manuscript received 7 April 2014, in final form 29 January 2015)

ABSTRACT

Wind turbine wakes in the atmosphere are three-dimensional (3D) and time dependent. An important question is how best to measure atmospheric wake properties, both for characterizing these properties observationally and for verification of numerical, conceptual, and physical (e.g., wind tunnel) models of wakes. Here a scanning, pulsed, coherent Doppler lidar is used to sample a turbine wake using 3D volume scan patterns that envelop the wake and simultaneously measure the inflow profile. The volume data are analyzed for quantities of interest, such as peak velocity deficit, downwind variability of the deficit, and downwind extent of the wake, in a manner that preserves the measured data. For the case study presented here, in which the wake was well defined in the lidar data, peak deficits of up to 80% were measured 0.6–2 rotor diameters (D) downwind of the turbine, and the wakes extended more than 11D downwind. Temporal wake variability over periods of minutes and the effects of atmospheric gusts and lulls in the inflow are demonstrated in the analysis. Lidar scanning trade-offs important to ensuring that the wake quantities of interest are adequately sampled by the scan pattern, including scan coverage, number of scans per volume, data resolution, and scan-cycle repeat interval, are discussed.

1. Introduction

Characterization of wind turbine wake properties and their downwind evolution is important for optimizing wind farm layouts and power output. Wake effects can produce reductions in power outputs integrated over wind farms and increases in fatigue loads on rotor blades, which can lead to premature failure of the hardware, as described by Crespo et al. (1999) and Vermeer et al. (2003). Turbine wakes have been studied using wind tunnel and computer simulations (e.g., Vermeer et al. 2003; Porté-Agel et al. 2011; Lu and Porté-Agel 2011; Churchfield et al. 2012), but the applicability of these results to real turbines can only be established through atmospheric measurements. In the atmosphere, wakes have been studied using instrumented towers (e.g., Magnusson and Smedman 1994; Elliott and Barnard 1990) and tethered balloons (e.g., Jacobs et al. 1984) at various downwind distances, and profiling remote sensing instrumentation, such as sodars and lidars (Högström et al. 1988; Barthelmie et al. 2003, 2010; Rhodes and Lundquist 2013). Recently, scanning remote sensing instrumentation—lidar and radar—have been used to study the structure of turbine wakes (Käsler et al. 2010; Clive 2011; Bingöl et al. 2010; Trujillo et al. 2011; Banta et al. 2011; Hirth et al. 2012; Hirth and Schroeder 2013; Iungo et al. 2013). An important aspect of using such remote sensors is how to obtain accurate, quantitative information on turbine wake properties.

In this note we use the three-dimensional (3D) scanning capability of a coherent, pulsed Doppler lidar system, the high-resolution Doppler lidar (HRDL), built and deployed by the Earth System Research Laboratory (ESRL) of the National Oceanic and Atmospheric

Corresponding author address: Robert M. Banta, NOAA/ESRL, 325 Broadway, Boulder, CO 80305.
E-mail: robert.banta@noaa.gov

DOI: 10.1175/JTECH-D-14-00078.1

Administration (NOAA). We present a case study illustrating the inherently 3D structure of a turbine wake, and we develop procedures for directly measuring several key wake properties. The measurements were taken as part of the Turbine Wake and Inflow Characterization Study (TWICS) in March–April 2011 (Smalikho et al. 2013; Aitken et al. 2014a,b).

2. Measurements

HRDL is a scanning, remote sensing instrument that measures aerosol backscatter and the wind component along the lidar beam. A description of HRDL and its specifications are given by Grund et al. (2001) and summarized in Table 1. The beam is steered by a two-mirror, azimuth–elevation scanner to map the along-beam, line-of-sight, or radial wind fields. Doppler lidar has been demonstrated to be an accurate technology to measure mean winds (Grund et al. 2001; Tucker et al. 2009, 2010; Pichugina et al. 2008, 2012; Kindler et al. 2007; Peña et al. 2008, 2009; Mann et al. 2010) and turbulent variances (Pichugina et al. 2008), with instantaneous root-mean-square (rms) uncertainties less than 20 cm s^{-1} and random instrument errors less than 5 cm s^{-1} for mean wind values averaged over time intervals of 1 min or more. Smoothing by HRDL's 30-m pulse volume, a minor effect on the bulk wake properties considered here, is neglected, and the radial wind velocities are treated as point values ascribed to the centroid of the sampling volume, as in Pichugina et al. (2008). HRDL has been used to study the structure of flows and turbulence at inland locations (Banta et al. 2002, 2003, 2006, 2013; Banta 2008; Pichugina et al. 2008; Pichugina and Banta 2010) and offshore aboard a research ship, using a custom-built motion-compensation system to remove ship and wave motions (Grund et al. 2001; Tucker et al. 2009, 2010; Pichugina et al. 2012). HRDL's high precision and narrow beam are significant advantages in studying turbine wakes.

To obtain data on wind flow and wake characteristics of a 2.3-MW wind turbine during the TWICS project, HRDL was deployed to the National Wind Technology Center (NWTC) test site (Clifton et al. 2013) of the National Renewable Energy Laboratory (NREL) south of Boulder, Colorado, located on the plains 5 km east of Colorado's Rocky Mountains. The wind turbine in the study had a hub height of 80 m and a rotor diameter D of 101 m. HRDL was sited 891 m to the west-northwest of the turbine at a slightly higher elevation, such that the lidar beam hit the turbine hub at an elevation angle of 4° and an azimuth of 130.55° measured clockwise from north. Wind flow at this site is often channeled through Eldorado Canyon (Kelley 2011; Banta et al. 1993, 1995, 1996; Clifton et al. 2013), providing prevailing westerly winds from a direction of 292°. The site experiences complex-terrain effects, such as enhanced turbulence night and day, that affect wake characteristics. Further details are presented in Smalikho et al. 2013 and Aitken et al. 2014b.

TABLE 1. HRDL instrument and scan properties. Pulse duration is between pulse-energy half-width points.

Lidar specifications	Value
Wavelength (μm)	2.02
Pulse energy (mJ)	2.0
PRF (Hz)	200
Pulses averaged	100
Effective PRF (Hz)	2
Pulse duration, length (ns, m)	200, 30
Range-gate interval (m)	30
Velocity precision (cm s^{-1})	<5
Minimum range (m)	190
Maximum range (km)	2–7 (typically 3)
Beam cross section at 2 km (cm)	<15

A three-phase scanning strategy was employed during TWICS. First, at the beginning of every half hour, full 360° conical scans at 1°, 5°, and 30° elevation documented the vertical profile of the horizontal wind using velocity–azimuth display (VAD) processing (Browning and Wexler 1968; Banta et al. 2002). The vertical spacing δz between velocity points in the vertical profile from a VAD calculation at 1° elevation is (30 m)(sin1°) = 0.52 m. At 5°, δz = 2.6 m, and at 30°, δz = 15 m. To accommodate this increase in δz in forming a single profile from all three scans, the radial velocity V_R versus azimuth data are collected into vertically stacked bins whose thicknesses Δz gently increase with z: $z(n) = an^b$, where n = 1, 2, 3, . . . , and z represents the midpoint of the nth bin. The values for a and b are chosen based on the elevation angles used in the VAD sequence. For the present TWICS analysis, a = 5 m and b = 1.35. The two mean wind components (either speed and direction or u and v) are then calculated within each vertical bin (of depth Δz) to form the profile. Note that this processing allows all data taken within the averaging period, including those from sector and vertical-slice scans, to be included in the bin averaging (Banta et al. 2002). VAD winds were used here to calculate ambient wind speeds and directions, which were then compared with inflow values estimated from the sector and vertical-slice scans, to assure that these estimates were consistent with the area-averaged profiles provided by the VAD technique.

Second, at other times in the 30-min scan series, when not performing VAD-type scans, the scans alternated between azimuth (or conical sector) scanning and elevation (or vertical slice) scanning to probe the wake

TABLE 2. Scan data for the two scan sequences analyzed.

Scan parameters						
Start time (UTC)	Type	Scan direction	Azimuth range	Elevation range	Scan speed	Angular step at 2 Hz
0411:22	Conical sector	Azimuth	115°–150°	0°, 2°, 4°, 6°	1.6° s^{-1}	0.8°
0412:53	Conical sector					
0414:22	Conical sector					
0415:52	Conical sector					
0417:21	Conical sector					
0307:12	Vertical slice	Elevation	125.5°, 127.5°, 129.5°, 131.5°	−1° to 12°	1.0° s^{-1}	0.5°
0307:29	Vertical slice					
0307:43	Vertical slice					
0307:59	Vertical slice					

structure. Sample scan patterns appear in Table 2. For this analysis the horizontal velocity component V_H of the lidar-measured radial velocity V_R was calculated as $V_H = V_R/\cos\theta$, where θ = elevation angle.

Third, vertical staring was performed for several minutes to measure vertical-velocity variance, which was used to give an estimate of daytime boundary layer depth. This note focuses on the interpretation of a wake during a 90-min period defined by two sets of such scans, as listed in Table 2.

Velocity deficits are quantified as deviations from a background flow, which can be determined in various ways. Here we choose the winds at hub height averaged over 2–5 rotor diameters (2*D*–5*D*) upwind of the turbine as the background flow. The precise manner of specification of the inflow is a topic of ongoing research. Figure 1 is a summary plot showing several time series of mean and turbulence quantities during one of the scan sequences analyzed in section 3. The background stability was weakly stable during the early evening hours, with 2–80 m and Richardson numbers (Ri) of 0.08–0.19 (Fig. 1d), as measured on an NWTC instrumented tower, referred to as the M2 tower, located at the west side of the NWTC (see Clifton et al. 2013).

3. Analysis of 3D wake properties

Low-elevation azimuth scans provide data over a sector of a shallow cone, revealing a wake's horizontal structure. A conical sector scan at $\theta = 2°$ elevation (Fig. 2a) shows a 3–4 m s^{-1} wake embedded in an 8 m s^{-1} background flow. At this wind speed, the turbine rotor would produce a significant thrust load, inducing a very energetic wake. The wake drifted with a mean wind not directly aligned with the lidar–turbine direction, meandering about the mean wind direction. Wind speed cross sections across the wake (Fig. 2b) reveal the peak wake deficit at each distance (asterisk). The location of these minimum values, plotted as black + signs on Fig. 2a, were not necessarily located symmetrically within the wake.

A useful way to visualize wake properties is to plot wind speed along radials in these sector scans as a function of distance outward from the lidar, as indicated by the colored rays in Fig. 2a. Wake properties inferred from these plots depend strongly on the azimuth of the radial chosen (Fig. 2c), because of wake meander and the slight crosswind angle of the beams. For example, in Fig. 2c the dark-blue curve represents velocity data along the radial at 129° azimuth from the lidar, indicating a short deficit region extending about 150 m (1½ rotor diameters or 1.5*D*) downwind from the rotor. The red curve (along 125° azimuth) shows strong velocity deficits extending downwind (1–6)*D*, and the magenta curve (119°) shows significant wake-deficit effects not starting until about 4*D* downwind. It is clear that proper characterization of the entire wake requires consideration of data from all available azimuths (Fig. 2d). In this plot, the minimum value at each range-gate distance (red symbols–line) quantifies the downwind extent of the wake, the peak value of the deficit, and the evolution of the wake deficit as a function of downwind distance.

Velocity deficits appearing at or even upwind of the rotor plane can be seen in Figs. 2b–d. Although plausible that these may represent actual flow retardation seen in the rotor upwind induction zone, this effect could also be partly due to turbine hardware intercepting the lidar pulse (see the appendix for a more detailed discussion), as described by Käsler et al. 2010. How best to deal with this effect is currently under investigation.

Elevation-scan (vertical slice) data may also be analyzed to provide a 3D image of the wake. It is often illustrative to interpolate data to constant heights, such as hub height or rotor top, before quantifying the range dependence of the velocity. A sample vertical-slice scan along one azimuth (Fig. 3a) extends from −1° to 12° elevation. Variations in wake magnitude and behavior

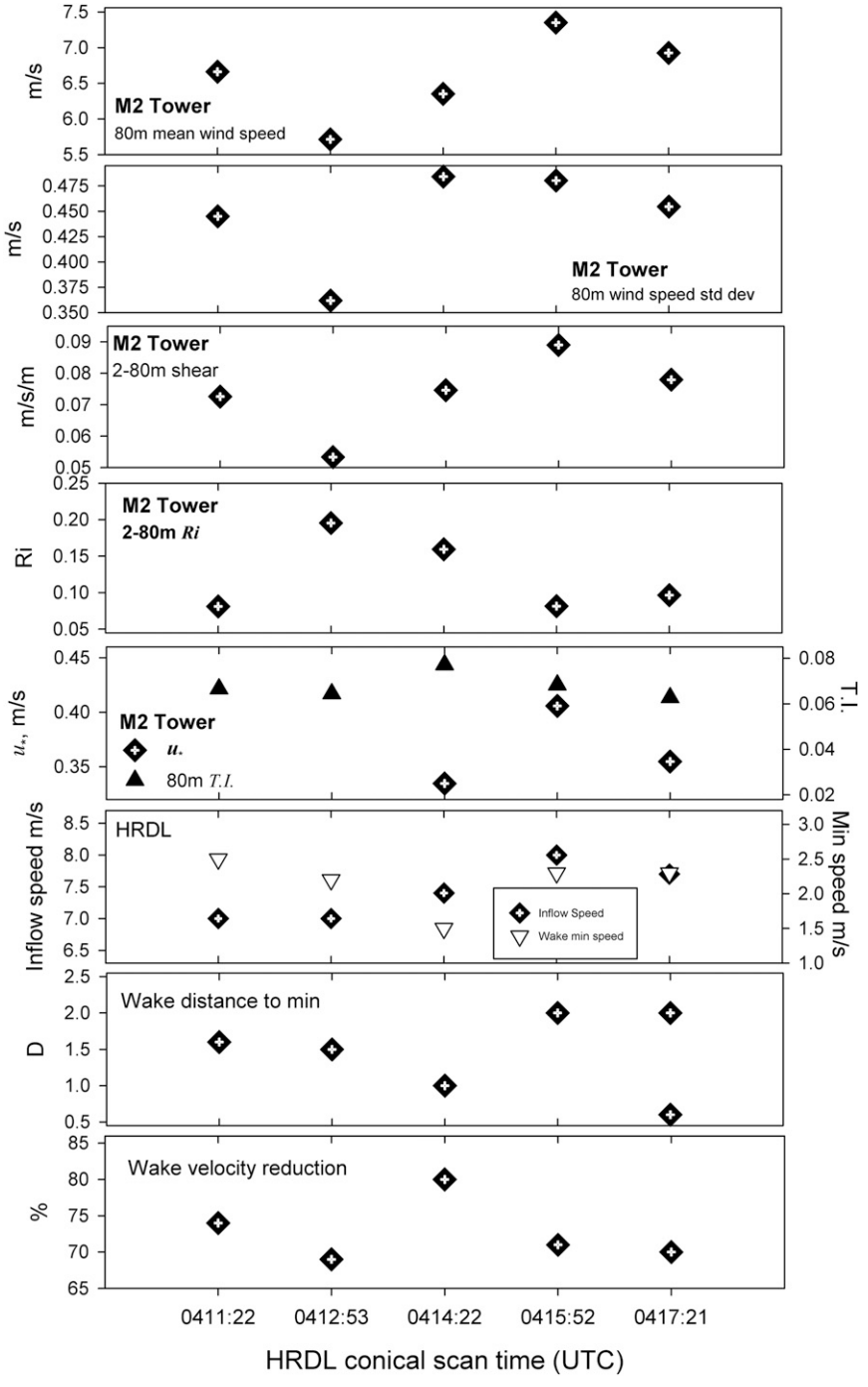

FIG. 1. Summary plot showing time series of data collected on the M2 tower approximately 1170 m directly upwind of the turbine. Mean wind speed and standard deviation were derived from a cup anemometer at the 80-m elevation. Mean vertical shear and friction velocity were calculated from the mean wind speed profiles measured by cup anemometers at heights of 2, 5, 10, 20, 50, and 80 m AGL. The Richardson number stability parameter was computed from the vertical shear and ambient air temperatures were measured at 2-, 50-, and 80-m heights. Wake properties summarized here were determined from HRDL scan data as described in section 3.

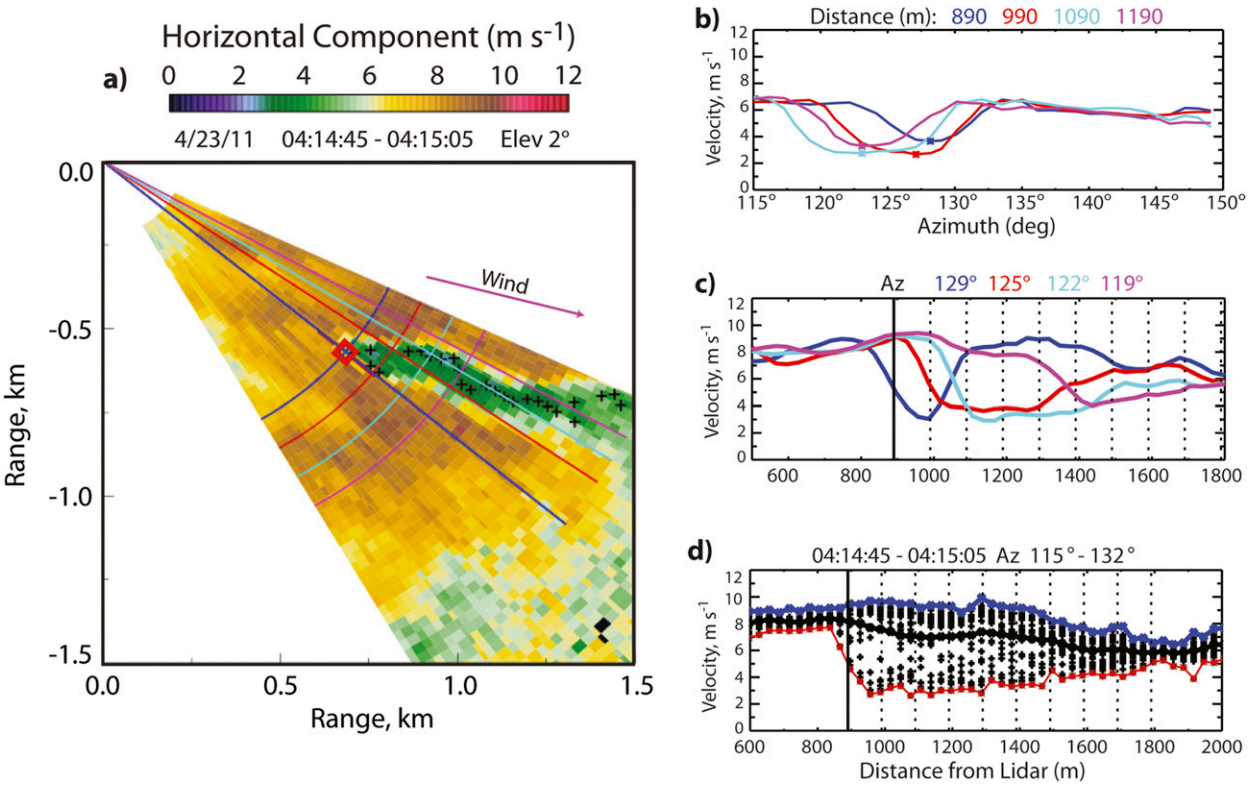

FIG. 2. (a) Conical sector scan performed at an elevation angle of 2° at 0414 UTC 23 Apr. The quantity V_H is color shaded from 0 to 12 m s^{-1}. Wind turbine location is shown by the red square (890 m from lidar), and the black plus signs (+) show the minimum velocity for each range-gate cross section in the wake [see (b)]. Purple arrow indicates observed mean wind direction, and area of reduced velocity downwind of the turbine is clearly seen on the plot. (b) The V_H along radial-arc cross sections at constant distance from the lidar. Individual range arc colors in (a) correspond to colors of curves here. (c) The V_H along individual azimuth rays as a function of range from lidar. The solid vertical line indicates HRDL position, and vertical dotted lines show intervals of 1D. Colors of radial-ray lines in (a) correspond to curve colors in this panel. Downwind distances have been corrected for the difference in azimuth angle between the lidar–turbine direction and the mean wind direction, which in this case is small. (d) The V_H plotted as a function of range as in (c) for *all rays* of data in the scan depicted in (a). Black line, showing mean values across the scan, indicates upwind inflow of 8 m s^{-1}. Red line, indicating minimum value across the scan, shows wake behavior, and blue line represents maximum velocity value across scan.

emerge at different heights, even within the rotor layer (Fig. 3b). Vertical profiles of horizontal wind speed at different distances from the turbine (Fig. 3c) show how the height of maximum deficit evolved downwind. The profile at 5D suggests the wake already dissipated, but we know from Fig. 2 that the wake actually persisted past this distance but moved out of this particular vertical plane. Thus, proper characterization of the wake behavior at a given range would require data from many sequential vertical-slice scans at incremented azimuths. Ideally this scan cycle would be performed quickly enough that the wake could be considered stationary (see section 4). During TWICS, vertical-slice scans were generally taken in a cycle of four scans (Fig. 4a), which was completed in <20 s. The sequence of Figs. 4b–e illustrates the vertical meander, ''looping'' behavior that the wakes sometimes displayed.

The variations seen in wake characteristics in the vertical imply that a wake cannot be completely characterized by a single-elevation conical sector scan (Fig. 2a), but that it requires collecting these scans at several elevations to capture wake properties such as peak deficit, which may occur at any height within a wake embedded in complex atmospheric flow (as opposed to steady inflow conditions of wind tunnels or many computer simulations). During TWICS, sector scans were taken in sequences or cycles, or ''stacks,'' of four elevations—0°, 2°, 4°, and 6° (Fig. 5a). Each of the four scans, including the horizontal 0°, show some evidence of wake, as illustrated in Fig. 5b. To account properly for the fact that wake properties of interest could occur in any of the scans, the analysis of Fig. 2d should be expanded to incorporate the flow information from all of the conical sector scan planes (Fig. 5c). The wake can be defined by the minimum value that occurs at any azimuth and any elevation for each given range.

Peak wind speed deficits could be quantified more simply by compiling the scan-volume velocity data and

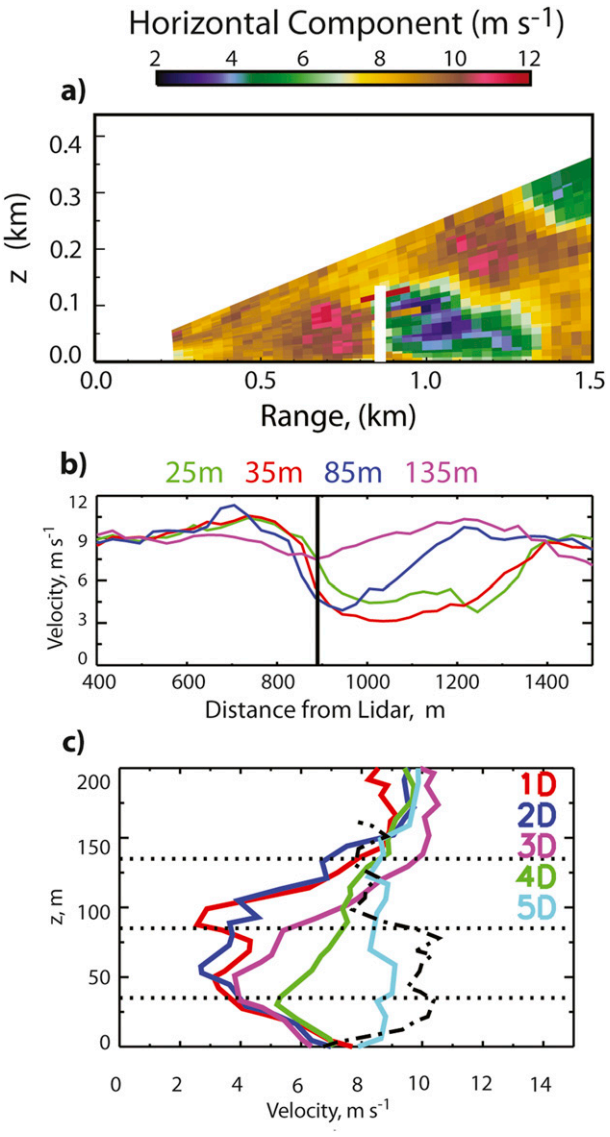

FIG. 3. (a) Vertical slice of radial velocity (color bar), obtained by scanning from −1° to 12° in elevation, showing approaching wind gust (red pixels) and the wake behind the turbine (blue pixels). Scan was performed at 0307 UTC 23 Apr, at an azimuth of 129.5° from the lidar. The mean VAD wind direction was from 300° just prior to this scan sequence. (b) The V_H as a function of distance from lidar, interpolated to four horizontal levels, as indicated by color coding, from the scan data shown in (a). Horizontal axis is the horizontal range from lidar (m) and vertical axis is horizontal wind speed (m s^{-1}). Flow deficit values upwind of turbine could be real flow retardation, or it could be a result of the interaction between the lidar pulse and the turbine hardware, as described in the appendix. (c) Vertical profiles of V_H at five distances downwind of wind turbine, as indicated by color coding. Vertical axis is height above lidar level and horizontal axis is wind speed (m s^{-1}). Plots represent nearly vertical profiles, considering the shallow elevation angles involved.

applying an extremum function (maximum or minimum, depending on the sign convention for the deficit). Advantages to performing the analysis presented here (Figs. 1d, 4c) include the visual aspect of seeing wake behavior as a function of range: being able to use this visual information to aid in the interpretation of wake behavior and to provide another level of quality control. For example, if the minimum value at a given range appeared anomalous, then it could be filtered. This approach also allows for flexibility in automating the procedure; for example, the second lowest value or the 5% lowest values could be used instead of the absolute minimum to define the wake. This kind of alternative wake criterion could prove useful in cases where the wake is less well defined, for example, if the atmosphere had low aerosol concentrations and therefore low lidar backscatter and noisier Doppler velocity data.

Values of several key wake properties for the 3D sample volumes considered here are given in Table 3 and Fig. 1. Shown are wake properties for five scan stacks taken over a 6-min period, which include those of Fig. 5 (middle stack, indicated by an asterisk). Wake lengths of $>11D$ agree with the wake lengths of $20D$ found by Hirth and Schroeder (2013). The data show significant variations over periods as short as minutes. Further, even though the 2° scan best characterized the wake overall, the 4° elevation scan often best quantified the *peak* deficit.

Scans also provide information about atmospheric variability, such as the 6° scan in Fig. 5b and the magenta curve in Fig. 5c, which show gusts (seen at 1200-m range) and lulls (at 1500-m range). By viewing the 6° five-scan series as an animation, these features can be tracked through the scan plane, indicating that they originated upwind of the turbine and lidar. Such nonstationary flow phenomena are common in the atmosphere and must be accounted for in defining wakes—for example, the lull, not the wake, represents the lowest wind speed at 1500 m in Fig. 5c. If an application requires ''instantaneous'' wake values from individual scan stacks, then such nonstationary anomalies need to be identified and disregarded. For other applications, where wake properties smoothed over several minutes may be more appropriate, wind values for the scans at each elevation angle (Fig. 5d) in all stacks can be averaged to produce a mean scan stack over the period of interest. The wake can then be defined as the lowest *mean* value at each range gate, effectively smoothing out nonstationary features.

4. Volume-scanning issues

Successful determination of wake properties depends primarily on how well the data capture quantities of

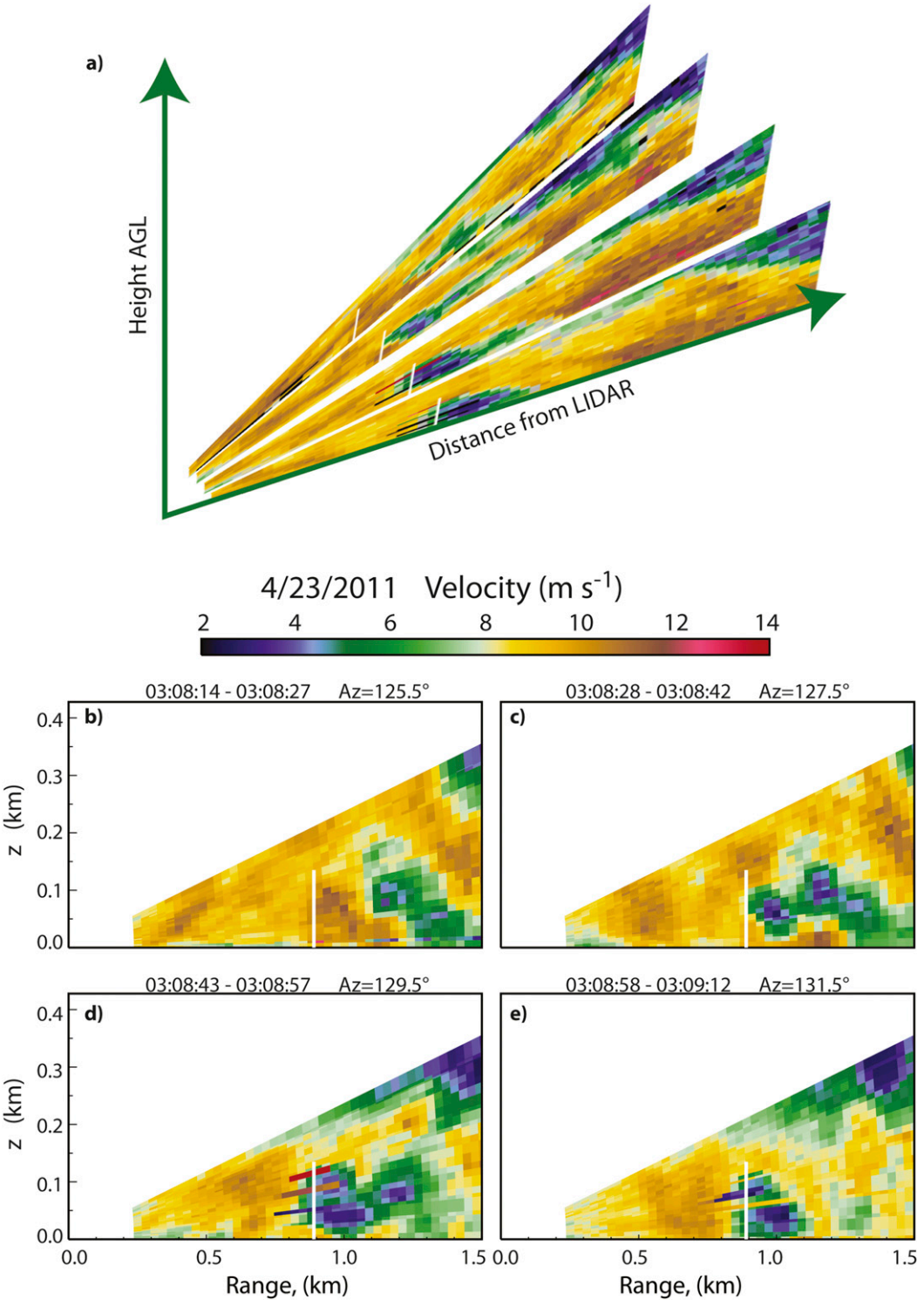

FIG. 4. (a) Sequence of four vertical-slice lidar scans of V_H taken at 0308 UTC 23 Apr. Turbine distance and height is indicated by white line on each scan. (b)–(e) Four scan panels showing detail for scans in (a), including vertical excursions of wake in cross sections (c) and (d). Turbine was sandwiched between scans (d) and (e). This scan cycle is typical of a vertical wake structure observed during the 90-min interval and was chosen to illustrate vertical-meander behavior [(b),(c)] sometimes evident in the TWICS dataset. Strips across the turbine in (d) and (e) represent where the turbine blade intercepts the lidar pulse.

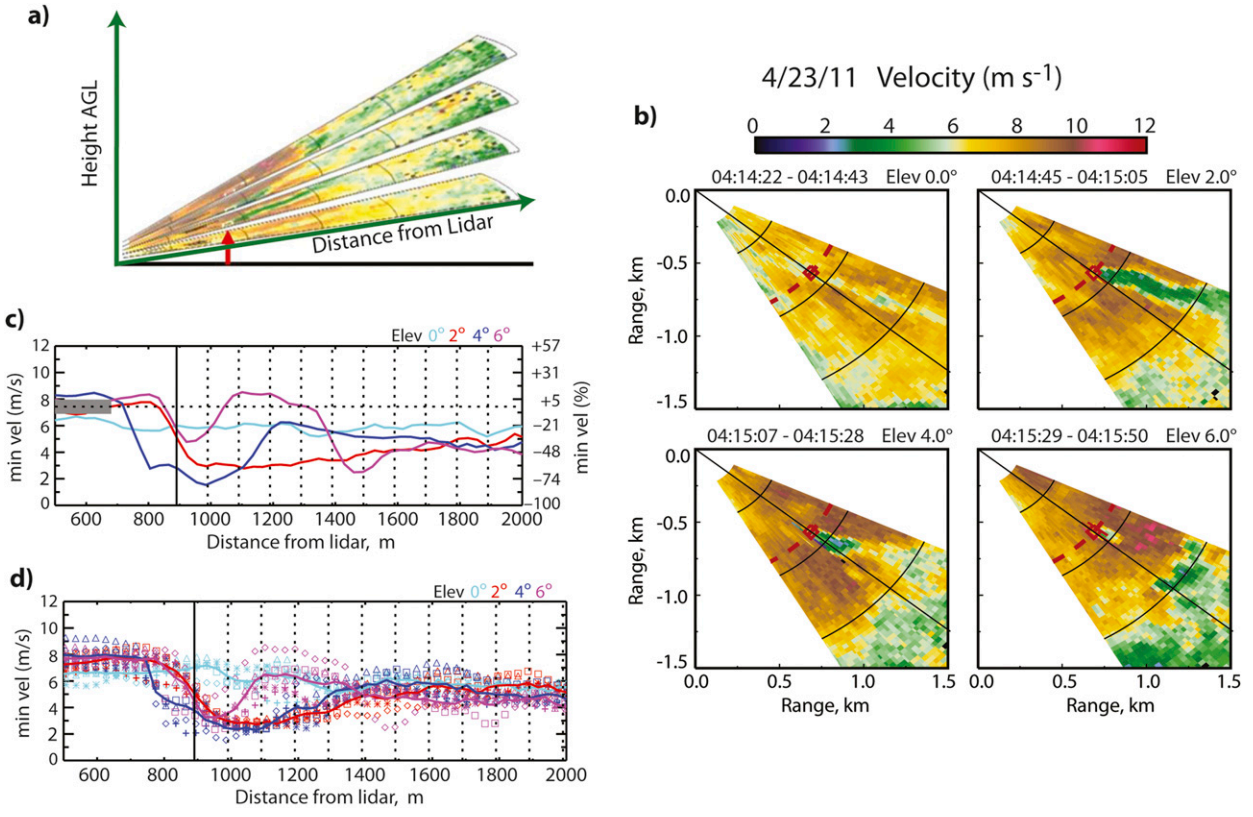

FIG. 5. (a) Orientation of vertically stacked conical sector scans of V_H taken at 0415 UTC with wind speeds color coded according to the scale to the right. (b) Detail of the four scan panels corresponding to sector scans in (a) at 0°, 2° (as in Fig. 1a), 4°, and 6° elevation, showing evidence of the wake on all four scans. (c) Curves show minimum V_H values as a function of range, determined in the same manner as the red curve in Fig. 1d, for each of the four scans in (a) and (b). Horizontal dotted line represents mean inflow value of 7.4 m s^{-1}, and vertical axis is labeled both in meters per second (left of axis) and in percent of inflow value (right of axis). Values at 6° elevation (magenta curve) reflect the effects of a wind gust at 1100–1200-m range and a lull in wind speed at 1500 m passing through the scan plane (such nonstationary effects occur at times in the atmosphere). The solid vertical line indicates HRDL position, and vertical dotted lines show intervals of 1D, as in Figs. 2c,d. (d) Minimum values for each scan as in (c), but for all five sector scan stacks between 0400 and 0420 UTC. Symbol colors show elevation angle of each minimum-value data point, and solid colored lines denote the mean of the five minimum values for each elevation. It is suggested that the line having the lowest value at each distance gives the best characterization of the mean wake behavior over the 6-min period by smoothing out nonstationary effects seen in individual scan stacks.

interest, which in turn depends on measurement considerations, such as sampling rate, sensitivity, and maximum downwind distance sampled—and on the scanning techniques employed. The scanning strategy involves compromises among the following issues:

- the extent or coverage of the scan volume
- the number of scans performed in a volume
- the scan-cycle repeat time
- the resolution of the data in the transverse or scanning direction, related inversely to the scanning speed (higher resolution requires slower scanning)

Maximizing the spatial density of data points in the atmospheric volume scanned, whether by increasing the number of scans in the volume or by slowing scanning speeds, is desirable to ensure the sampling will not miss an important value, such as the peak deficit. But these specifications also increase the time required to complete a single measurement volume. Flow structures evolve between the first and last scans in the volume, so that shorter scan-cycle repeat times are desired to capture the instantaneous structure of the wake. During TWICS, wake properties were observed to change over periods as short as a few minutes (Table 3). The individual cycles or stacks of four conical sector scans (Fig. 5a) for probing the horizontal wake structure took <2 min each, such that the five-stack series took <8 min. The four elevation (vertical slice) scan cycles required <20 s each.

Various scan strategies or procedures can be used to sample the wake. Elevation (vertical slice) scans elucidate the vertical structure, although each scan cycle may

TABLE 3. Wake properties for the series of five consecutive scan-stack cycles starting at 0411 UTC. Wake widths and lengths have been determined as recovery to within 10% of mean inflow speed.

Scan start time (UTC)	Inflow speed ($m\,s^{-1}$)	Minimum speed ($m\,s^{-1}$)	Inflow (%)	Reduction (%)	Distance to min	Scan angle of min speed (°)	Width at 1*D*, 2*D*, 3*D*, 4*D* (m)	Wake length
0411:22	7.0	2.5	36	74	1.6*D*	4		>11*D*
0412:54	7.0	2.2	31	69	1.5*D*	4		>11*D*
0414:22*	7.4	1.5	20	80	1.0*D*	4		>11*D*
0415:52	8.0	2.3	29	71	2.0*D*	4		>11*D*
0417:21	7.7	2.3	30	70	0.6, 2.0*D*	4, 6		>11*D*
Mean	7.4	2.3	31	69	1.5*D*	4	236, 286, 254, 341	>11*D*

* The scan sequence was analyzed in Figs. 1 and 4.

not span the entire horizontal extent of the wake in a short enough time to be useful. Current sampling capabilities—an *effective* pulse repetition frequency (PRF) of 2 Hz (200-Hz PRF averaged over 100 pulses: cf. Table 1)—suggest azimuth (conical sector) scanning can best define the horizontal extent of a wake, although the vertical structure may not be optimally represented in the data. When Doppler lidar technology advances to where accurate Doppler velocities can be obtained at effective rates exceeding 20 Hz with equivalent sensitivity, elevation scanning may become more advantageous; more vertical-slice scans could be performed in the time now required for a few such scans. This procedure would exploit the vertical resolution of elevation scans, but the scan cycle could cover the horizontal extent of the wake with future more-rapid sampling rates. Using current technology in TWICS, we alternated between azimuth and elevation sector-volume scanning to monitor any unexpected structure that could affect interpretation of the data.

Carefully conceived scan strategies are critical to ensure a dataset that adequately samples the wake. Having obtained the dataset, the question becomes, what is the best way to analyze it? The procedures described in section 3 have the advantage that the values obtained are actually measured values, so that to the extent that the peak deficits and other quantities are represented in the dataset, this procedure can extract the best estimate of them.

5. Conclusions

Turbine wakes are inherently 3D, time-dependent entities. The present case study illustrates this nature by probing the wake of an operating turbine in the real, nonstationary atmosphere. It demonstrates the importance of taking these variabilities into account in acquiring and analyzing the datasets. Two critical aspects of using measurement data to study wakes or other atmospheric phenomena can be singled out: planning beforehand and interpretation of the results afterward. The planning of a field program includes designing the data acquisition (including scanning) strategies, which depends on understanding the nature of wakes as well as the capabilities of the instrumentation used. The interpretation of the results by modelers, turbine designers, and wind farm planners happens after the data have been acquired, reduced, and analyzed. If the dataset was not properly taken and analyzed, then the results will have uncertainties and errors that could negate the apparent findings. The analysis approach described here extracts quantities of interest, such as wake extent or peak deficit, without alteration of the data by smoothing or fitting.

The case presented here was of a well-defined wake, as a result of adequate aerosol concentrations and resulting strong lidar signal. During periods of low aerosol concentrations or other conditions that may produce noisier data, the wake may be less distinct. In such cases, analysis algorithms that smooth the data or curve-fitting algorithms may improve the ability to estimate wake quantities (Aitken et al. 2014b). Reference datasets and procedures are needed to evaluate how well such algorithms perform when wakes are well defined, to assess the reliability of the algorithms. These high-precision measurement datasets and high-confidence procedures for determining wake properties, such as those presented here, are also needed for evaluating how well numerical model output (Porté-Agel et al. 2011; Churchfield et al. 2012; Aitken et al. 2014a; Mirocha et al. 2014) and wind tunnel results (e.g., España et al. 2011) apply to turbine wakes in the atmosphere (Shaw et al. 2009).

Acknowledgments. We thank the turbine manufacturer's staff for its facilitation of observational periods and Matthew Aitken for his thoughtful manuscript review. This work was sponsored by the U.S. Department of Energy's Wind and Hydropower Technologies program, under the direction of the Office of Energy Efficiency and Renewable Energy (Interagency Agreement DE-NA0000900).

APPENDIX

Effects of Lidar Pulse Interception by Hard Targets

The transmitted energy profile of a lidar pulse in time or space may be thought of as Gaussian along its (line of sight) propagation path. The pulse length—30 m in this case—indicates the distance between the half-power (or 1/*e*, depending on definition) points along the pulse, where the peak and the vast majority of the pulse energy lies. When the small amount of pulse energy outside this range encounters normal atmospheric scatterers, the amount of backscattered energy returning to the lidar is negligibly small, as compared with the returns from the peak of the pulse. However, when this tiny amount of energy ahead of or behind the nominal 30-m pulse hits a strongly reflective hard target, such as a turbine rotor blade, the amount of energy bounced back to the lidar can easily exceed weak atmospheric backscatter from the central portions of other pulses that do not hit the blade. The result can sometimes be seen dramatically as radial strips of anomalous velocities appearing in adjacent range gates ahead of or behind the turbine location, as seen in Figs. 2a and 3d,e. This effect may be seen in one, two, or occasionally more range gates from the hard target. At other times, and more subtly, the laser pulse may graze a blade, or else only some of the laser shots making up HRDL's 2-Hz averages (cf. Table 1) of the lidar "beam" may strike the rotor, influencing the mean wind values calculated at 2 Hz. Thus, using current data reduction and analysis procedures, velocities in the vicinity of the turbine should be interpreted with caution. These effects are currently under further investigation to explore ways to eliminate these artifacts. It is important to also note, however, that the vast majority (probably $> 99\%$) of lidar beams used in the analysis presented here does not pass near the turbine blades, and thus the data from these beams are free of the hardware-interception effects just described.

REFERENCES

Aitken, M. L., B. Kosović, J. D. Mirocha, and J. K. Lundquist, 2014a: Large eddy simulation of wind turbine wake dynamics in the stable boundary layer using the Weather Research and Forecasting Model. *J. Renewable Sustainable Energy,* **6,** 033137, doi:10.1063/1.4885111.

——, J. K. Lundquist, R. M. Banta, and Y. L. Pichugina, 2014b: Quantifying wind turbine wake characteristics from scanning remote sensor data. *J. Atmos. Oceanic Technol.,* **31,** 765–787, doi:10.1175/JTECH-D-13-00104.1.

Banta, R. M., 2008: Stable-boundary-layer regimes from the perspective of the low-level jet. *Acta Geophys.,* **56,** 58–87, doi:10.2478/s11600-007-0049-8.

——, L. D. Olivier, and P. H. Gudikson, 1993: Sampling requirements for drainage flows that transport atmospheric contaminants in complex terrain. *Radiat. Prot. Dosim.,* **50,** 243–248.

——, ——, W. D. Neff, D. H. Levinson, and D. Ruffieux, 1995: Influence of canyon-induced flows on flow and dispersion over adjacent plains. *Theor. Appl. Climatol.,* **52,** 27–42, doi:10.1007/BF00865505.

——, ——, P. H. Gudikson, and R. Lange, 1996: Implications of small-scale flow features to modeling dispersion over complex terrain. *J. Appl. Meteor.,* **35,** 330–342, doi:10.1175/1520-0450(1996)035<0330:IOSSFF>2.0.CO;2.

——, R. K. Newsom, J. K. Lundquist, Y. L. Pichugina, R. L. Coulter, and L. Mahrt, 2002: Nocturnal low-level jet characteristics over Kansas during CASES-99. *Bound.-Layer Meteor.,* **105,** 221–252, doi:10.1023/A:1019992330866.

——, Y. L. Pichugina, and R. K. Newsom, 2003: Relationship between low-level jet properties and turbulence kinetic energy in the nocturnal stable boundary layer. *J. Atmos. Sci.,* **60,** 2549–2555, doi:10.1175/1520-0469(2003)060<2549:RBLJPA>2.0.CO;2.

——, ——, and W. A. Brewer, 2006: Turbulent velocity-variance profiles in the stable boundary layer generated by a nocturnal low-level jet. *J. Atmos. Sci.,* **63,** 2700–2719, doi:10.1175/JAS3776.1.

——, W. A. Brewer, R. M. Hardesty, Y. L. Pichugina, J. K. Lundquist, N. D. Kelley, and J. Mirocha, 2011: Enhancing energy production by wind farms. *SPIE Newsroom,* doi:10.1117/2.1201107.003800.

——, ——, N. D. Kelley, W. A. Brewer, and R. M. Hardesty, 2013: Wind-energy meteorology: Insight into wind properties in the turbine rotor layer of the atmosphere from high-resolution Doppler lidar. *Bull. Amer. Meteor. Soc.,* **94,** 883–902, doi:10.1175/BAMS-D-11-00057.1.

Barthelmie, R. J., L. Folkerts, F. Ormel, P. Sanderhoff, P. Eecen, O. Stobbe, and N. M. Nielsen, 2003: Offshore wind turbine wakes measured by sodar. *J. Atmos. Oceanic Technol.,* **20,** 466–477, doi:10.1175/1520-0426(2003)20<466:OWTWMB>2.0.CO;2.

——, and Coauthors, 2010: Quantifying the impact of wind turbine wakes on power output at offshore wind farms. *J. Atmos. Oceanic Technol.,* **27,** 1302–1317, doi:10.1175/2010JTECHA1398.1.

Bingöl, F., J. Mann, and G. C. Larsen, 2010: Light detection and ranging measurements of wake dynamics part I: One-dimensional scanning. *Wind Energy,* **13,** 51–61, doi:10.1002/we.352.

Browning, K. A., and R. Wexler, 1968: The determination of kinematic properties of a wind field using Doppler radar. *J. Appl. Meteor.,* **7,** 105–113, doi:10.1175/1520-0450(1968)007<0105:TDOKPO>2.0.CO;2.

Churchfield, M. J., S. Lee, J. Michalakes, and P. J. Moriarty, 2012: A numerical study of the effects of atmospheric and wake turbulence on wind turbine dynamics. *J. Turbul.,* **13,** N14, doi:10.1080/14685248.2012.668191.

Clifton, A., S. Schreck, G. Scott, N. Kelley, and J. K. Lundquist, 2013: Turbine inflow characterization at the National Wind Technology Center. *J. Sol. Energy Eng.,* **135,** 031017, doi:10.1115/1.4024068.

Clive, P. I., L. Dinwoodie, and F. Quail, 2011: Direct measurement of wind turbine wakes using remote sensing. *Proc. EWEA 2011,* Brussels, Belgium, European Wind Energy Association, 1502. [Available online at http://proceedings.ewea.org/annual2011/allfiles2/1502_EWEA2011presentation.pdf.]

Crespo, A., J. Hernandez, and S. Frandsen, 1999: Survey of modelling methods for wind turbine wakes and wind farms. *Wind Energy,* **2,** 1–24, doi:10.1002/(SICI)1099-1824(199901/03)2:1<1::AID-WE16>3.0.CO;2-7.

Elliott, D. L., and J. C. Barnard, 1990: Observations of wind turbine wakes and surface roughness effects on wind flow variability. *Sol. Energy,* **45,** 265–283, doi:10.1016/0038-092X(90)90012-2.

España, G., S. Aubrun, S. Loyer, and P. Devinant, 2011: Spatial study of the wake meandering using modelled wind turbines in a wind tunnel. *Wind Energy,* **14,** 923–937, doi:10.1002/we.515.

Grund, C. J., R. M. Banta, J. L. George, J. N. Howell, M. J. Post, R. A. Richter, and A. M. Weickmann, 2001: High-resolution Doppler lidar for boundary-layer and cloud research. *J. Atmos. Oceanic Technol.,* **18,** 376–393, doi:10.1175/1520-0426(2001)018<0376:HRDLFB>2.0.CO;2.

Hirth, B. D., and J. L. Schroeder, 2013: Documenting wind speed and power deficits behind a utility-scale wind turbine. *J. Appl. Meteor. Climatol.,* **52,** 39–46, doi:10.1175/JAMC-D-12-0145.1.

——, ——, W. S. Gunter, and J. G. Guynes, 2012: Measuring a utility-scale turbine wake using the TTUKa mobile research radars. *J. Atmos. Ocean. Technol.,* **29,** 765−771, doi:10.1175/JTECH-D-12-00039.1.

Högström, U., D. N. Asimakopoulos, H. Kambezidis, C. G. Helmis, and A.-S. Smedman, 1988: A field study of the wake behind a 2 MW wind turbine. *Atmos. Environ.,* **22,** 803–820, doi:10.1016/0004-6981(88)90020-0.

Iungo, G. V., Y.-T. Wu, and F. Porté-Agel, 2013: Field measurements of wind turbine wakes with lidars. *J. Atmos. Oceanic Technol.,* **30,** 274–287, doi:10.1175/JTECH-D-12-00051.1.

Jacobs, E. W., N. D. Kelley, H. E. McKenna, and N. J. Birkenheuer, 1984: Wake characteristics of the MOD-2 wind turbine at Medicine Bow, Wyoming. Solar Energy Research Institute Tech. Paper SERI/TP-214-2587, 10 pp. [Available online at http://www.nrel.gov/docs/legosti/old/2567.pdf.]

Käsler, Y., S. Rahm, R. Simmet, and M. Kuhn, 2010: Wake measurements of a multi-MW wind turbine with coherent long-range pulsed Doppler wind lidar. *J. Atmos. Oceanic Technol.,* **27,** 1529–1532, doi:10.1175/2010JTECHA1483.1.

Kelley, N. D., 2011: Turbine–turbulence interaction: The basis for the development of the TurbSim stochastic simulator. NREL Tech. Rep. NREL/TP-5000-52353, 299 pp. [Available online at http://www.nrel.gov/docs/fy12osti/52353.pdf.]

Kindler, D., A. Oldroyd, A. MacAskill, and D. Finch, 2007: An eight month test campaign of the Qinetiq ZephIR system: Preliminary results. *Meteor. Z.,* **16,** 479–489, doi:10.1127/0941-2948/2007/0226.

Lu, H., and F. Porté-Agel, 2011: Large-eddy simulation of a very large wind farm in a stable atmospheric boundary layer. *Phys. Fluids,* **23,** 065101, doi:10.1063/1.3589857.

Magnusson, M., and A.-S. Smedman, 1994: Influence of atmospheric stability on wind turbine wakes. *Wind Eng.,* **18,** 139–152.

Mann, J., A. Peña, F. Bingöl, R. Wagner, and M. S. Courtney, 2010: Lidar scanning of momentum flux in and above the atmospheric surface layer. *J. Atmos. Oceanic Technol.,* **27,** 959–976, doi:10.1175/2010JTECHA1389.1.

Mirocha, J., B. Kosovic, M. L. Aitken, and J. K. Lundquist, 2014: Implementation of a generalized actuator disk wind turbine model into WRF for large-eddy simulation applications. *J. Renewable Sustainable Energy,* **6,** 013104, doi:10.1063/1.4861061.

Peña, A., C. B. Hasager, S.-E. Gryning, M. Courtney, I. Antoniou, and T. Mikkelsen, 2008: Measurements and modelling of the wind speed profile in the marine atmospheric boundary layer. *Bound.-Layer Meteor.,* **129,** 479–495, doi:10.1007/s10546-008-9323-9.

——, C. B. Hasagar, S.-E. Gryning, M. Courtney, I. Antoniou, and T. Mikkelsen, 2009: Offshore wind profiling using light detection and ranging measurements. *Wind Energy,* **12,** 105–124, doi:10.1002/we.283.

Pichugina, Y. L., and R. M. Banta, 2010: Stable boundary-layer depth from high-resolution measurements of the mean wind profile. *J. Appl. Meteor. Climatol.,* **49,** 20–35, doi:10.1175/2009JAMC2168.1.

——, ——, N. D. Kelley, B. Jonkman, S. C. Tucker, R. K. Newsom, and W. A. Brewer, 2008: Horizontal-velocity and variance measurements in the stable boundary layer using Doppler lidar: Sensitivity to averaging procedures. *J. Atmos. Oceanic Technol.,* **25,** 1307–1327, doi:10.1175/2008JTECHA988.1.

——, ——, W. A. Brewer, S. P. Sandberg, and R. M. Hardesty, 2012: Doppler lidar–based wind-profile measurement system for offshore wind-energy and other marine boundary layer applications. *J. Appl. Meteor. Climatol.,* **51,** 327–349, doi:10.1175/JAMC-D-11-040.1.

Porté-Agel, F., Y.-T. Wu, H. Lu, and R. Conzemius, 2011: Large-eddy simulation of atmospheric boundary layer flow through wind turbines and wind farms. *J. Wind Eng. Ind. Aerodyn.,* **99,** 154–168, doi:10.1016/j.jweia.2011.01.011.

Rhodes, M. E., and J. K. Lundquist, 2013: The effect of wind turbine wakes on summertime Midwest atmospheric wind profiles. *Bound.-Layer Meteor.,* **149,** 85–103, doi:10.1007/s10546-013-9834-x.

Shaw, W. J., J. K. Lundquist, and S. J. Schreck, 2009: Research needs for wind resource characterization. *Bull. Amer. Meteor. Soc.,* **90,** 535–538, doi:10.1175/2008BAMS2729.1.

Smalikho, I. N., V. A. Banakh, Y. L. Pichugina, W. A. Brewer, R. M. Banta, J. K. Lundquist, and N. D. Kelley, 2013: Lidar investigation of atmosphere effect on a wind turbine wake. *J. Atmos. Oceanic Technol.,* **30,** 2554–2570, doi:10.1175/JTECH-D-12-00108.1.

Trujillo, J.-J., F. Bingöl, G. C. Larsen, J. Mann, and M. Kühn, 2011: Light detection and ranging measurements of wake dynamics. Part II: Two-dimensional scanning. *Wind Energy,* **14,** 61–75, doi:10.1002/we.402.

Tucker, S. C., W. A. Brewer, R. M. Banta, C. J. Senff, S. P. Sandberg, D. C. Law, A. M. Weickmann, and R. M. Hardesty, 2009: Doppler lidar estimation of mixing height using turbulence, shear, and aerosol profiles. *J. Atmos. Oceanic Technol.,* **26,** 673–688, doi:10.1175/2008JTECHA1157.1.

——, and Coauthors, 2010: Relationships of coastal nocturnal boundary layer winds and turbulence to Houston ozone concentrations during TexAQS 2006. *J. Geophys. Res.,* **115,** D10304, doi:10.1029/2009JD013169.

Vermeer, L. J., J. N. Sørensen, and A. Crespo, 2003: Wind turbine wake aerodynamics. *Prog. Aerosp. Sci.,* **39,** 467–510, doi:10.1016/S0376-0421(03)00078-2.